The microseismic response at the In Salah Carbon Capture and Storage (CCS) site

Anna L. Stork*, James P. Verdon, J.-Michael Kendall

School of Earth Sciences, University of Bristol, Wills Memorial Building, Queen's Road, Bristol BS8 1RJ, UK

A B S T R A C T

In 2004, injection of carbon dioxide (CO_2) to be stored at depth began at the In Salah Carbon Capture and Storage (CCS) site and a pilot microseismic monitoring array was installed in 2009. The In Salah project presents an unusual dataset since it is the first major non-Enhanced Oil Recovery (EOR) CCS project to be monitored for microseismicity. This paper outlines an extensive seismological study using a range of techniques, relying mainly on data from a single three-component geophone. Important information is derived from the data, such as event locations, event magnitudes and fracture characteristics, that could be used in real-time to regulate the geomechanical response of a site to CO_2 injection. The event rate closely follows the CO_2 injection rate, with a total of 9506 seismic events detected. The locations for a carefully selected subset of events are estimated to occur at or below the injection interval, thereby ruling out fault or fracture activation caused by CO_2 migration at shallow depths. A very small number of events (11) with less well-constrained locations may have occurred above the injection interval. However, there is no microseismic evidence that these events are correlated with CO_2 injection and we suggest they are caused by stress transfer rather than CO_2 migration into the caprock. The observed maximum moment magnitude, $M_w = 1.7$, is consistent with estimated fracture dimensions at the injection depth. Fracture orientation estimated using shear-wave splitting analysis is approximately NW-SE, in agreement with fracture orientations inferred from logging data. During periods of high injection rates the degree of anisotropy increases slightly and then falls back to original values when injection rates fall. This implies the CO_2 is opening pre-existing fractures which then close as pressure decreases.

This an important proof-of-concept study that proves the value of microseismic monitoring of CCS projects, even with a limited array. We thus recommend that microseismic monitoring arrays are installed prior to CO_2 injection at future CCS sites to enhance our understanding by making baseline and comparative studies possible. This would also provide real-time monitoring of the geomechanical response to injection, allowing operators to modify injection parameters and to help ensure the safe operation of a project.

1. Introduction

Carbon Capture and Storage (CCS) projects, where CO_2 is injected into the ground to be stored at depth, is one technology with the potential to reduce anthropogenic CO_2 emissions to mitigate global warming. For the technology to be safe and effective, this CO_2 must remain trapped for thousands of years. However, few large-scale projects have so far come on-line and many questions remain about the geological and geomechanical response to the injection of millions of tons of supercritical CO_2 at up to several kilometres depth. One particular concern for CO_2 storage security

is the potential for such projects to induce earthquakes (Zoback and Gorelick, 2012; Verdon, 2014). Induced seismicity may result from the reactivation of pre-existing faults or fractures, or by generating new fracture networks. The injection of CO_2 increases pore pressure around an injection site which reduces frictional resistance to fault slip and effective stress. Small stress perturbations in an already critically stressed crust could therefore activate nearby faults, resulting in pathways for CO_2 leakage. Similarly, there is an increased risk to safe storage if injection pressures exceed the value required to produce new fracture networks extending into the overburden.

Understanding a site's geomechanical response to CO_2 injection is key to the success of a project because without this knowledge the potential for CO_2 leakage is unidentified. Even though only a small number of CCS projects exist, it has been observed that the

* Corresponding author. Tel.: +44(0)1179545698.
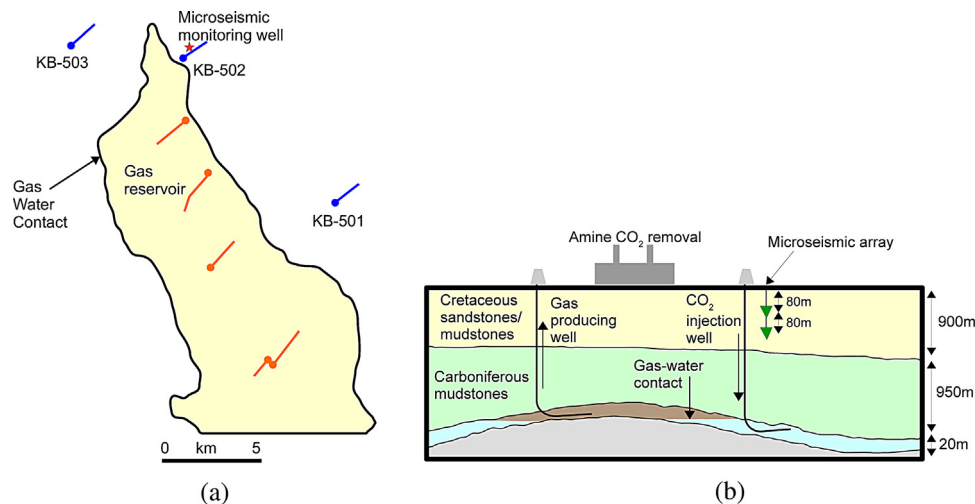*E-mail address:* anna.stork@bristol.ac.uk (A.L. Stork).

Fig. 1. (a) Schematic illustration of the Krechba field showing the location of the injector (blue) and gas-producing (orange) wells. The star indicates the location of the microseismic monitoring well and the horizontal extent of the gas–water contact is given by the black line. (b) Schematic illustration of the geology of the Krechba field. Gas is produced from and the CO_2 is injected into a ∼20 m thick reservoir at 1850–1900 m deep. The positions of the geophones used in this study are also indicated by the green triangles. (For interpretation of the references to color in this figure legend, the reader is referred to the web version of this article.)

geomechanical response to injection is very different depending on the geological setting (Verdon et al., 2013). The Weyburn field, Canada and the Sleipner field in Norway are two major CCS projects that inject ≥1 million tonnes (Mt) of CO_2 per year. At Weyburn CO_2 has been injected for enhanced oil recovery (EOR) since 2000, with some increase in pore pressure (15–20 MPa) and a small number of induced seismic events, ∼100 between 2003 and 2010 (Verdon et al., 2011). To date the Sleipner field in Norway is the site of the world's largest non-EOR CCS project where around 14 million tonnes (Mt) of CO_2 have been sequestered since 1996 and where pressures are reported to have remained close to pre-injection levels (Chadwick et al., 2012). This makes significant geomechanical deformation and seismic activity at the site unlikely. In contrast, injection of <1 Mt of CO_2 at the Decatur CCS demonstration project in the Illinois basin resulted in the detection of 1000s of microseismic events (Coueslan et al., 2013). In this study we focus on the response at the In Salah storage site to CO_2 injection using a variety of seismological techniques. We review the microseismic activity at the site to investigate the possibility that CO_2 injection 2009–2011 caused fracturing in the reservoir. In addition, we look at how real-time microseismic data might be used to infer CO_2 migration and help regulate the geomechanical response of a reservoir to injection. The techniques applied here are also important and relevant to controlling site response in other industries that require fluid injection (e.g., wastewater injection; hydraulic fracturing and enhanced geothermal stimulation).

2. The In Salah CO_2 storage site

The In Salah CO_2 storage project at the gas-producing Krechba field in Algeria is a pioneering onshore CCS project that began injection in 2004. Between 2004 and 2011, nearly 4 Mt of CO_2 was injected by three injection wells, KB-501, KB-502 and KB-503 (Fig. 1a; Ringrose et al., 2013). The CO_2 was injected into the ∼20 m thick downdip water leg of the gas reservoir at ∼1.9 km depth (Fig. 1b; Mathieson et al., 2010). The reservoir is overlain by ∼950 m Carboniferous mudstones, siltstones, and limestones which, in turn, is overlain by Cretaceous sandstone deposits (Ringrose et al., 2009). This thickness of caprock makes it a good site for CO_2 storage. However, the porosity and permeability of the storage rocks are low relative to other large-scale projects, ∼10% and 10 mD respectively (Eiken et al., 2011). To measure the site performance in terms

of injectivity and storage capacity a suite of geophysical and geochemical monitoring methods were put in place (Mathieson et al., 2011).

The response of the reservoir to CO_2 injection has been observed using two key geophysical technologies: InSAR (Interferometric Synthetic Aperture Radar) and 3D seismic surveys. Surface deformation of up to several cm was observed above the injection wells through InSAR. Inversion of this data places deformation due to volume and fracture aperture changes at reservoir depth around the injection wells (Vasco et al., 2010; Rucci et al., 2013). The dimensions and depth are in agreement with results from a 2009 3D seismic survey concluding that injection has activated a deep fracture zone extending NW of KB-502, several hundred metres wide and extending about 150 m above the reservoir (Rutqvist, 2012). The fracture zone is aligned parallel to the dominant NW-SE fracture orientation and perpendicular to the minimum compressive principal stress (Iding and Ringrose, 2010; Rutqvist, 2012), supporting the idea that these observations are the result of fracture opening in the lower caprock rather than opening or reactivation of a large-fault.

3. Microseismic instrumentation and data

In 2009 a pilot microseismic monitoring array was installed in well KB-601, almost directly above the horizontal extension of injector KB-502 (Fig. 1). Six three-component (3-C) 15 Hz geophones between 80 m and 500 m deep were connected and recorded continuous data at 500 Hz until June 2011 (Oye et al., 2013). Unfortunately, due to technical issues (e.g., non-functioning channels, cabling problems and malfunctioning GPS units), it has only been possible to orientate and confidently process the data from one 3-C geophone, the uppermost instrument at 80 m deep. In addition the vertical component of the geophone at 160 m deep provides reliable data.

We use the two reliable vertical components of data to detect events using cross-correlation methods similar to those described in Forghani-Arani et al. (2013). Initially the short-term average (STA) recorded amplitude to long-term average (LTA) amplitude ratio is calculated using rolling time-windows. For the given velocity model (Oye, *pers. comm.* and Fig. 2) and assuming events occur below the microseismic array, we estimate the expected travel-time difference between *P*-phases arriving from below at the two
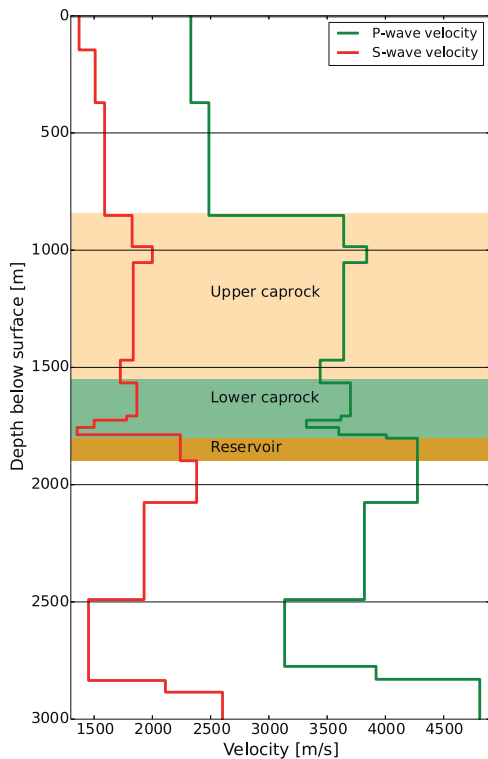
Fig. 2. The 1D layered *P*- and *S*-wave velocity models used in the finite difference modelling and ray-tracing experiments to estimate event locations. The depth intervals of reservoir, lower caprock and upper caprock are also indicated.

geophones to be 0.02–0.05 s. Where the STA/LTA ratio exceeds a given threshold on both traces within the estimated travel-time difference, a potential event is identified. Through trial and error a threshold of 2.4 was selected as providing the best balance, maximising event detection while minimising false triggers. The *P*-arrival times are picked at the times of maximum cross-correlation between the STA/LTA for the two vertical components (Fig. 3). *S*-phases are then picked manually. Using this method, 9506 microseismic events were detected between August 2009 and June 2011, 1000s of events more than have been detected using a conventional STA/LTA trigger or master-event cross-correlation (Oye et al., 2013; Goertz-Allmann et al., 2014).
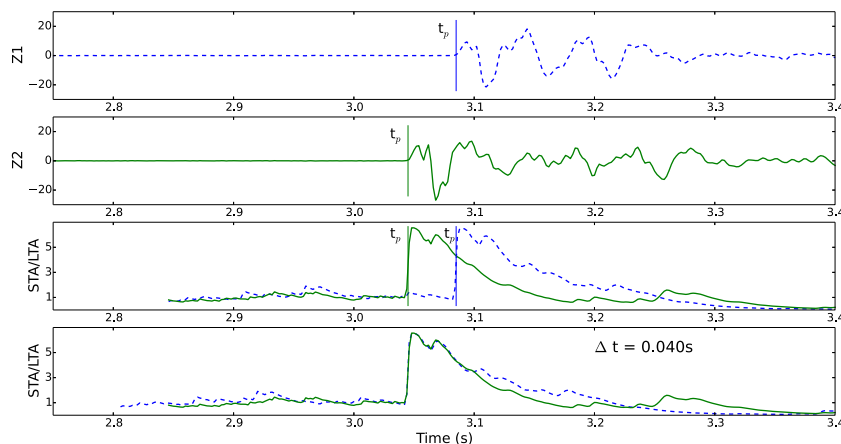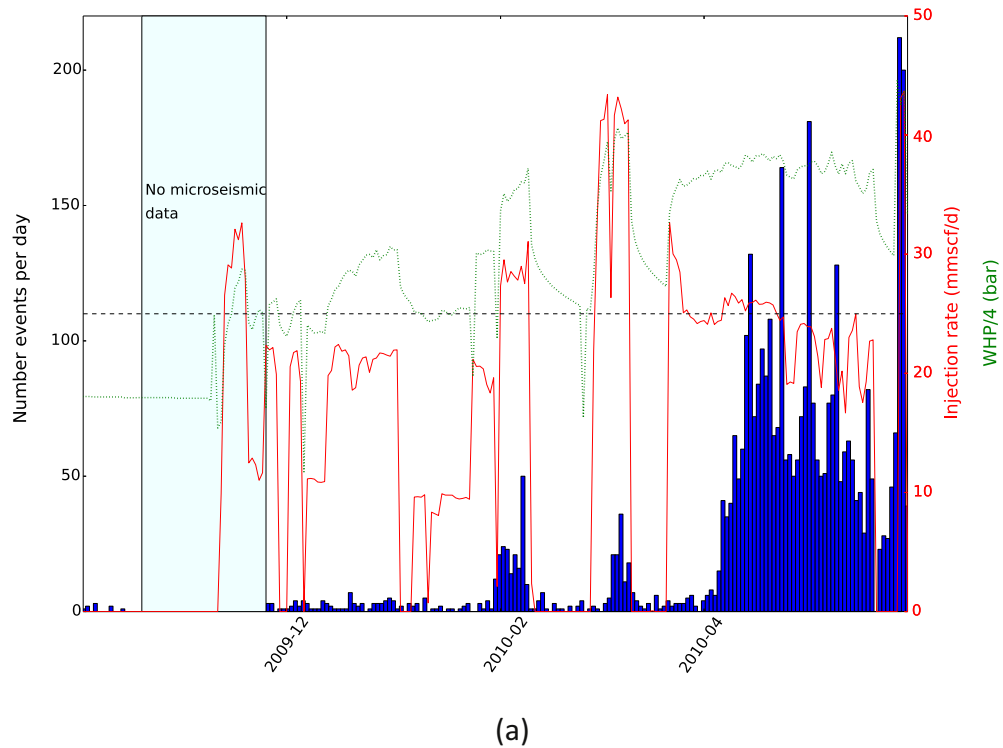
P-arrival particle motion is linear in the direction of propagation so to obtain an estimate of the direction (the azimuth and inclination) to the source from the receiver we perform *P*-wave particle motion analysis, following De Meersman et al. (2006). The azimuth is defined as the angle clockwise from North and the inclination is defined as the angle from vertical downwards. For quality-control we measure the linearity of the *P*-wave particle motion (De Meersman et al., 2006; Claassen, 2001) and the event location results presented below include only the 1610 events with linearity $\geq$0.95 (the linearity is 1 for perfectly linearly polarised *P*-waves and 0.5 for circularly polarised particle motion). We use a variety of analyses in treatment of the data which are outlined in the relevant sections.
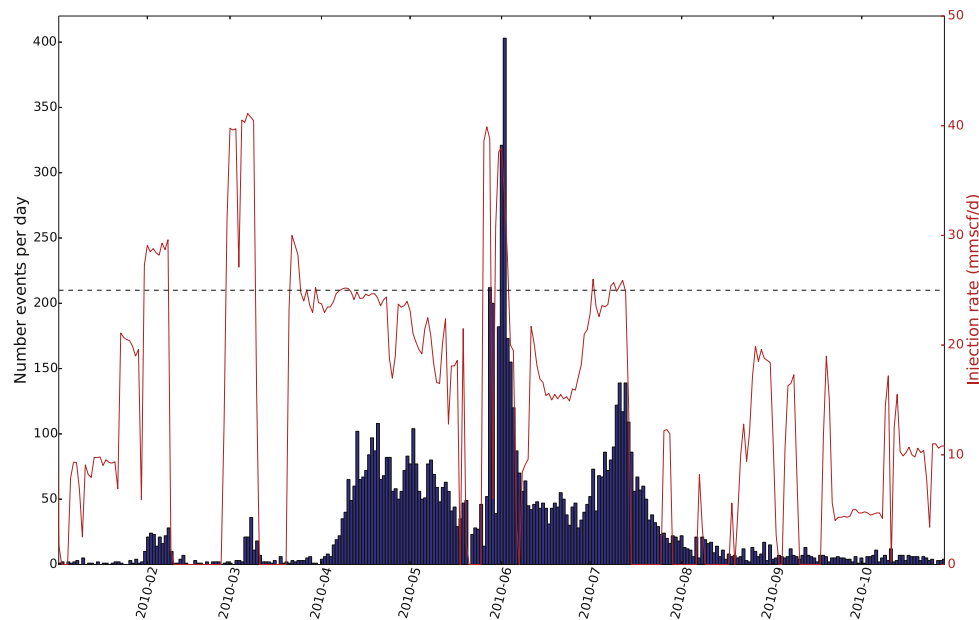
4. Data analysis

A suite of techniques is applied to the data to gain maximum information from the single three-component geophone data. Many standard techniques are unavailable for a single instrument but we adapt and apply appropriate techniques to gain significant and useful information from the dataset.

4.1. Event rate

The picking algorithm developed specifically for this data resulted in 9506 *P*-arrival picks and following this 6280 *S*-arrivals are picked by hand. The observed event rate correlates with the injection rate at well KB-502, illustrated by the data in Fig. 4. The event rate increases, and rises to a maximum of 400 events/day, when the injection rate exceeds 25 million standard cubic feet per day (mmscf/d), as is the case on several occasions between February and July 2010. There is a delayed response of up to 14 days in the onset of seismicity following an increased injection rate. This could be an example of what is known as the Kaiser effect, which states that there is an absence of brittle failure in a material until the load has exceeded the previously applied maximum load (Kaiser, 1959). Once the injection rate falls from these high rates to zero, the number of detected events immediately begins to drop and returns to <10 events/day within 1–7 days. This behaviour suggests that even though high injection rates result in a large number of events, the microseismicity can be controlled by adjusting the injection rate. The difference in the absolute numbers of events in February–March 2010 compared to April–June 2010 is thought to be result of the injection history. In 2009 only

Fig. 3. Illustration of the picking procedure. The vertical component seismograms for the two geophones (Z1 and Z2) are shown in the upper two panels. Below these are the STA/LTA functions for these seismograms and in the bottom panel the STA/LTA functions are shifted for maximum cross-correlation. A *P*-arrival, t_p, is picked where the STA/LTA function is above the given threshold on both traces if the time shift, Δt, is within the expected time difference for arrivals at the two geophones (0.02–0.05 s).

(a)

(b)

Fig. 4. Histograms showing (a) the number of events detected early in the monitoring period (October 2009–May 2010) and (b) the number of events detected per day in 2010. There is no microseismic data available for November and December 2010. The injection rate at well KB-502 is shown by the red line in million standard cubic feet per day, with the 25 mmscf/d level indicated by the dashed line. The green line is well-head pressure/4 in bar. (For interpretation of the references to color in this figure legend, the reader is referred to the web version of this article.)

small quantities of CO_2 were injected at KB502 and the well-head pressure was low (∼70 bar, Fig. 4a). Once injection restarts it takes some time for the pressure to build up in the surrounding formation and following a sustained period of high well-head pressures in April 2010 (Fig. 4a) the event rate dramatically increased, presumably as the pressure increased at distance from the injection point.

4.2. Event clustering

If differences in arrival times of multiple seismic phases, for example *P*- and *S*-waves, are available this enables the source-station distance to be calculated, provided a velocity model is available for the region in question. Using *P*- and *S*-arrival times, the overwhelming majority of events recorded at the In Salah site
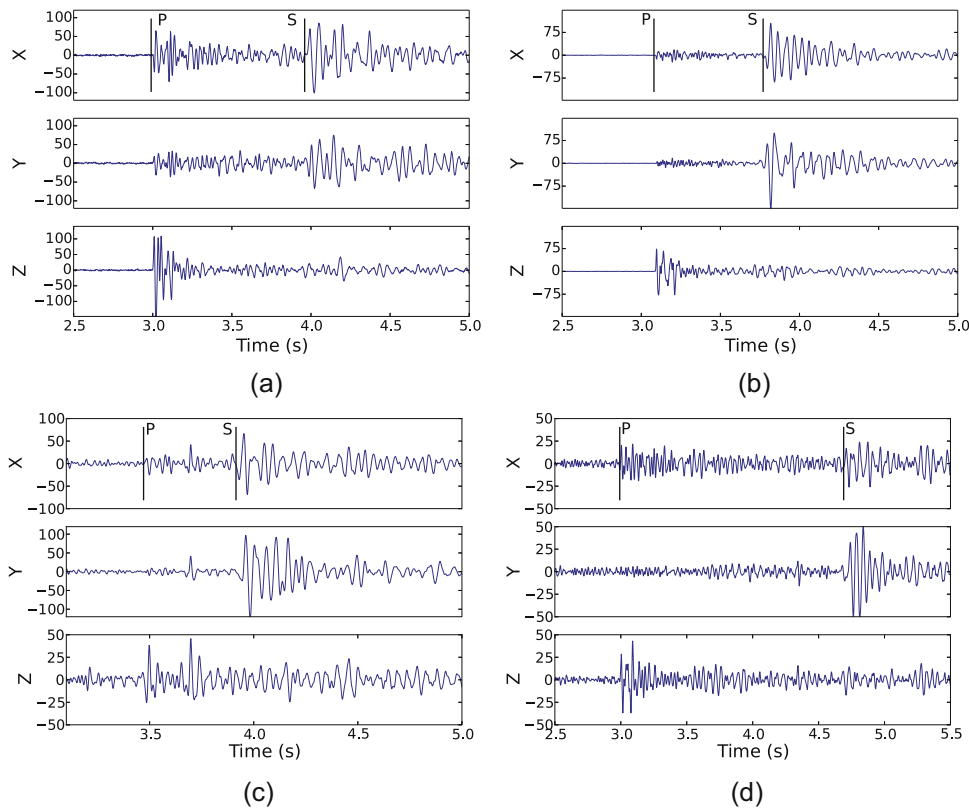
Fig. 5. Example seismograms for events in (a) Cluster 1 ($t_{sp} \sim 0.95$ s), (b) Cluster 2 $t_{sp} \sim 0.68$ s), and events with t_{sp} times (c) shorter and (d) longer than those observed for Clusters 1 and 2. The two horizontal (X and Y) and the vertical (Z) components are given.
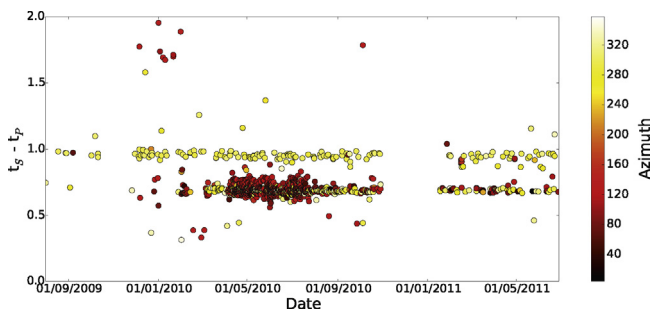

Fig. 6. t_{sp} times measured for events throughout the monitoring period. The colour indicates the azimuth of the P-arrival. (For interpretation of the references to color in this figure legend, the reader is referred to the web version of this article.)

can be separated into two distinct clusters that occur throughout the monitoring period and example seismograms are shown in Fig. 5a and b. These occur in groups with almost constant $S - P$ arrival times, t_{sp}, at ∼0.95 s and ∼0.68 s, illustrated in Fig. 6 and subsequently named Clusters 1 and 2, with 136 and 1226 events respectively. At times, usually during periods of high injection rates (>25 mmscf/d), Cluster 2 spreads out to $t_{sp} = 0.68 \pm 0.04$ s. If these events are repeating events, occurring at the same location and with the same mechanism, then the waveforms within a cluster will be highly correlated. Cluster 1 shows such characteristics with >75% of the events in Cluster 1 having similar waveforms with correlation coefficients >0.9 (Fig. 7a and b). The variation within Cluster 2 is greater, as would be expected because there is more variation in t_{sp} times in this cluster, but it contains two sub-clusters with correlation coefficients >0.9 that include most of the events in the cluster (Fig. 7c). These clusters show no evolution with time and

events occur throughout the monitoring period. It seems a large portion of the observed seismicity is repeating events, occurring at two locations and the similarity between waveforms within the clusters suggests they have very similar mechanisms.

The azimuth and inclination measured for these events (Fig. 8) shows Cluster 2 events occur almost directly below the array and along a trend with an average azimuth of 109°–289°. These directions are consistent with the events occurring on a NW-SE oriented fracture zone offset slightly to the West of the array. The events observed here are more widely distributed than the four tight clusters of events reported by (Goertz-Allmann et al., 2014). We suggest that this is a result of the differences between picking algorithms since the arrivals identified in this study do not require any correlation with previously observed events.

4.3. Event locations

To gain a full understanding of the movement of injected CO_2 the location of any microseismicity is required. The extent of microseismic activity is often taken to represent the extent of hydraulic stimulation (e.g., Maxwell et al., 2002; Delépine et al., 2004) although microseismicity can often occur through stress transfer rather than directly being caused by the presence of fluids (Orlecka-Sikora et al., 2009; Schoenball et al., 2012). The occurrence of microseismicity in the cap rock is a particular concern for CCS sites if this indicates the activation of faults and fractures that allows CO_2 to migrate towards the surface. We therefore use observed t_{sp} times and directional information (the azimuth and inclination of recorded P-waves) to estimate the location of some events and identify any sequences of microseismicity that could indicate the migration of CO_2 into the caprock.
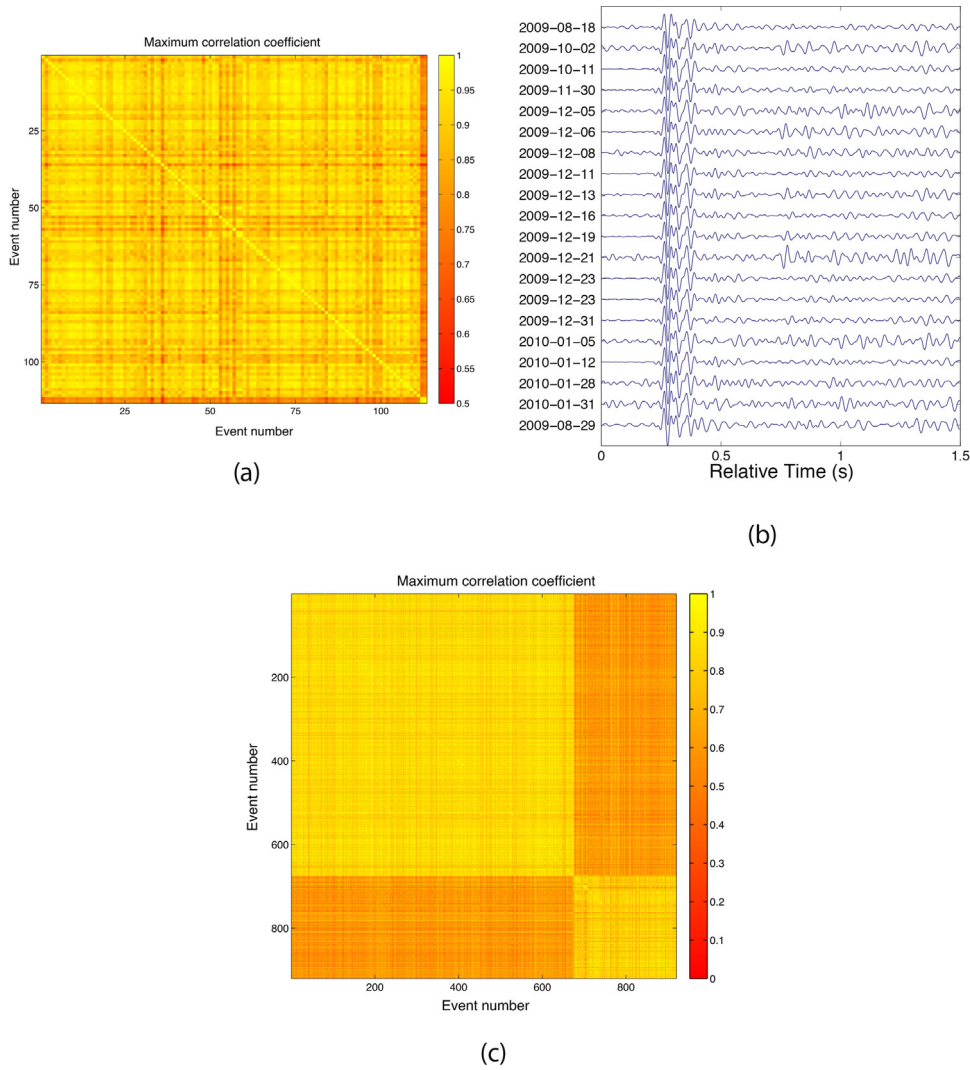
(a)

(b)

(c)

Fig. 7. (a) Correlation matrix for vertical component seismograms for events in Cluster 1 with correlation coefficients >0.9; (b) vertical waveforms for 20 of these events; and (c) correlation matrix for vertical component seismograms for events in Cluster 2 with correlation coefficients >0.9.
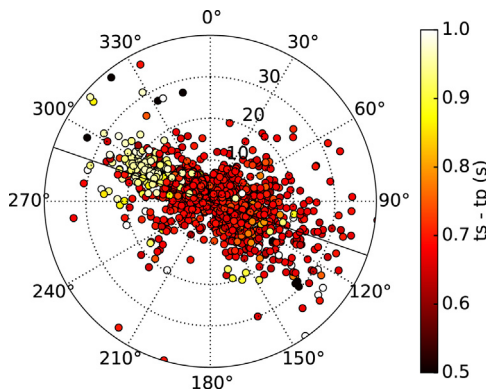

Fig. 8. Estimated azimuth (angular coordinate) and inclination (radial coordinate) of *P*-arrivals coloured by t_{sp} times. Results for arrivals with linearity ≥0.95 are shown. The average azimuth is indicated by the line 109°–289°. (For interpretation of the references to color in this figure legend, the reader is referred to the web version of this article.)

Since we have data from only one observation point, estimating accurate hypocentres for the observed events is difficult. There are many uncertainties in our observations. For example, our estimates of station-source azimuth and inclination contain measurement

and systematic errors due to the presence of noise and ray-bending in a layered velocity model.

To quantify the difference between observed inclinations, i_o, and the geographical inclination from receiver to the hypocentre, i_g, we carry out finite difference modelling using E3D, a 3-D elastic seismic wave propagation code (Larsen and Grieger, 1998) and a 1-D layered velocity model (Oye, *pers. comm.*; Fig. 2). From the synthetic waveforms we estimate the difference between observed and geographical incidences, $i_o - i_g$. We do this for a range of t_{sp} times using a grid of locations estimated using an eikonal solver (Fig. 9) and find that, for 0.60 s<t_{sp}<0.85 s, $i_g - i_o < 5°$ for $i_o < 15°$.

Using the criteria $i_o < 15°$ we estimate locations for 1214 events based on our measured azimuths, inclinations and the event location grid illustrated in Fig. 9. The estimated depth and horizontal distance of the events from the monitoring well give no indication that seismic activity becomes shallower with time or moves above the reservoir into the lower caprock (Fig. 10). The red colours in Fig. 10 represent events that occurred during the first half of 2010 when the injection rate and event rate were high and the spread in the estimated depths is ~600 m. Later in the sequence, in 2011 (day > 500), the events are restricted to a range in depths of ~250 m. Although absolute depths are difficult to determine here due to errors in the velocity model and the number of instruments, relative depths show that high injection rates do appear to stimulate
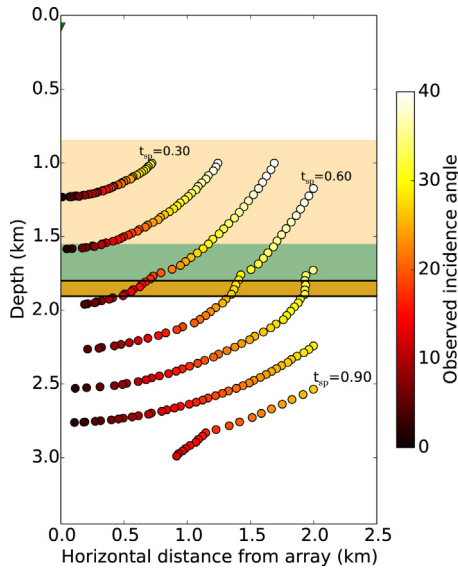
Fig. 9. Event depths and horizontal distances from the observation well for different t_{sp} times, estimated using E3D. The colours represent the inclination of the *P*-arrival measured from the synthetic waveforms. The caprock and reservoir layers are shaded as in Fig. 2 and the approximate injection interval is between the two thicker black lines at ~1.9 km deep. (For interpretation of the references to color in this figure legend, the reader is referred to the web version of this article.)
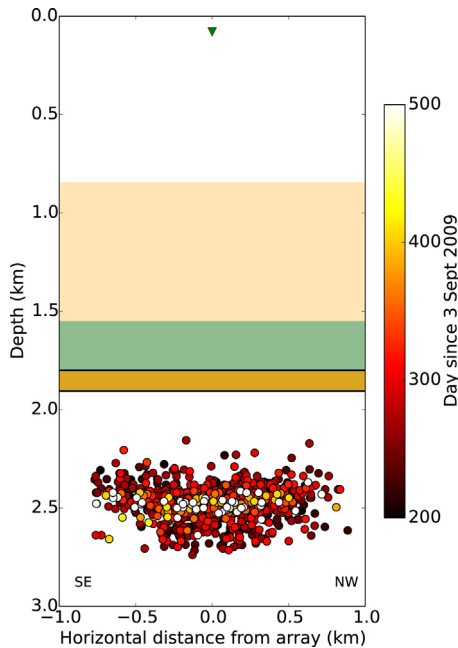

Fig. 10. Estimated depth and horizontal distance of events from observation well. Locations are projected onto a SE-NW plane. The colours indicate the time of the event in number of days since the earliest plotted event. Locations are estimated for events with $i_o < 15°$, linearity ≥ 0.95 and signal-to-noise ratio >3.0. The caprock and reservoir layers are shaded as in Fig. 2 and the approximate injection interval is between the two thicker black lines at ~1.9 km deep. The green triangle indicates the location of the geophone used in the analysis. (For interpretation of the references to color in this figure legend, the reader is referred to the web version of this article.)

a larger area to become seismically active. We do not observe any systematic shortening of t_{sp} times over time this suggests that there is no systematic migration of seismicity through the cap rock. This is reassuring for the containment of CO_2. We do observe a small number of events (11) with shorter t_{sp} times (<0.5 s) (Fig. 6). These do not satisfy our criteria to estimate locations but their significance is discussed below.
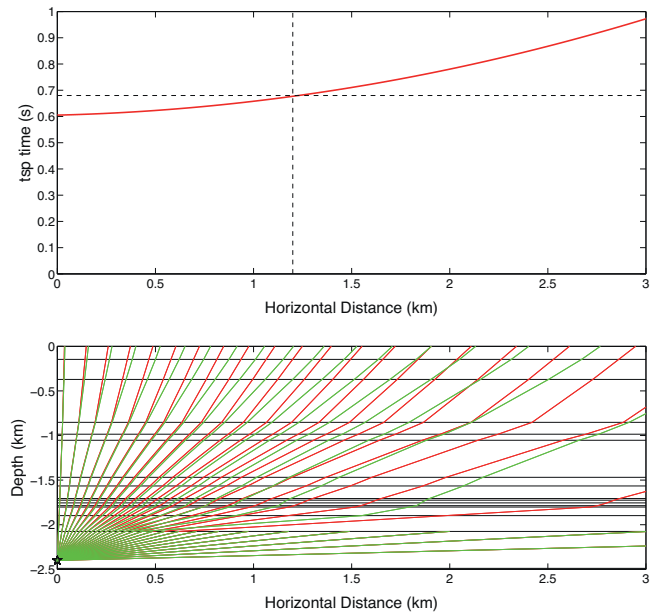

Fig. 11. Raytracing results for *P*- (red) and *S*-waves (green) (lower panel) and t_{sp} times as a function of distance (upper panel), estimated using the provided isotropic 1-D velocity model and a source at 2.4 km deep (star). (For interpretation of the references to color in this figure legend, the reader is referred to the web version of this article.)

To provide additional evidence for the approximate locations obtained through finite-difference modelling we conduct a ray-tracing exercise. The results from ray-tracing through the isotropic 1-D velocity model using the method of Kendall and Thomson (1989) show that events with hypocentres at 2.4 km depth and 1.2 km horizontal distance from the array (Fig. 11).

To estimate errors in our reported locations we tested the effect of the velocity model on the travel-times and, for example, we locate Cluster 2 up to 450 m shallower if the velocity model is 10% slower overall, if the near surface layer is 20% slower or if the model is anisotropic (see Stork et al., 2015 for a detailed description). This would place the events in this cluster between 1.65 km – 2.25 km deep and therefore extending up to 150 m unto the lower caprock. As an estimate of the error in horizontal distances from the array we take the maximum horizontal distance between grid points in Fig. 9, this is 174 m when $t_{sp} = 0.60$s near 0° incidence. Event locations obtained using the two methods, finite difference modelling and ray-tracing, agree within the estimated errors.

Overall, the results for the estimated location of Cluster 2 show that the seismicity occurred at depths over a range of ~600 m at or below the injection interval and at azimuths from the monitoring well consistent with the activation of a pre-existing wide fracture zone at the injection depth and extending into the lower caprock (as reported by Iding and Ringrose (2010) and Rutqvist (2012)) with events occurring on similarly oriented fractures within the zone. An inaccurate velocity model significantly affects seismic event locations and if the velocity model is 10% slower this would imply that the events extend into the lowermost 150 m of the caprock, consistent with the previous fracture zone interpretation. An anisotropic fractured medium may also affect interpretation of the data.

We note that a few events occur outside the two main clusters and example seismograms are shown in Fig. 5. We find 11 events with 0.31 s $<t_{sp}< 0.5$ s (Fig. 6 and example seismograms in Fig. 5c). According to our model locations in Fig. 9 these events are between 1.1 km and 1.8 km deep but, as with all locations reported here, there are significant uncertainties in these locations. The events occur over the whole monitoring period and there is no correlation
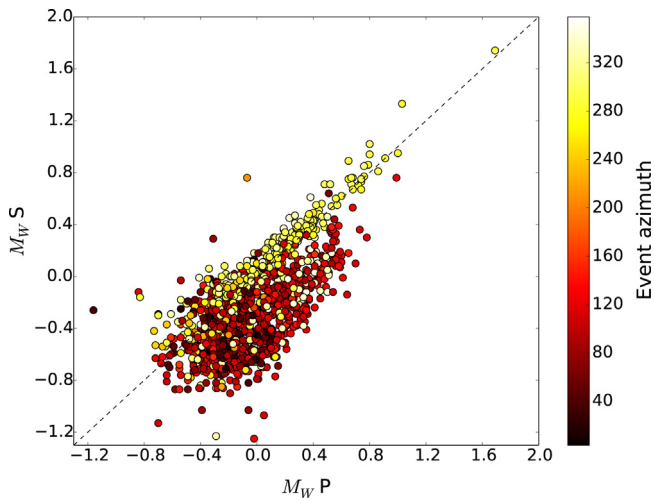
Fig. 12. Estimated M_w for P- and S-arrivals. Events are coloured by azimuth. (For interpretation of the references to color in this figure legend, the reader is referred to the web version of this article.)

with injection and no evidence that observed t_{sp} are becoming shorter with time. We therefore suggest that these events do not indicate the presence of CO_2 at shallower depths but that they are simply isolated individual events caused by stress transfer.

In addition we identify 12 events with $1.5\,s < t_{sp} < 2.2\,s$ (example seismograms in Fig. 5b). The estimated station-source azimuths for 11 of these are consistent with the events originating in the vicinity of injection well KB-501. This implies that we detect a few microseismic events associated with injection at KB-501. A more spatially extensive microseismic network would have been necessary to know this for certain.

4.4. Event magnitudes

With one 3-C geophone we are only able to obtain approximate moment magnitude, M_w, values. However, we estimate seismic moment, M_0, for events satisfying the conditions linearity >0.95 and $i_g - i_o < 5°$ with a signal-to-noise ratio >3.0 using

$$M_0 = \frac{4\pi\rho v^3 r\Omega_0}{R}, \tag{1}$$

where R is the P- or S-wave radiation pattern correction term, ρ is the rock density, v is the P- or S-wave velocity at the source, r is the source-receiver distance and Ω_0 is the low frequency level of the amplitude spectrum. We have no estimate of focal mechanism solutions so we use average radiation pattern corrections (0.44 for P-waves and 0.60 for S-waves: Boore and Boatwright, 1984) and Ω_0 is taken directly from the amplitude spectrum at frequencies <50 Hz. The spectra are corrected for geometrical spreading and intrinsic attenuation for P- and S-waves, Q_p and Q_s, respectively. Since we are unable to make a reliable estimate of Q directly we perform 1000 iterations of the calculation using Q-values taken from a random uniform distribution with $Q_p = 100$–400 and $Q_s = 100$–400. We also allow for some uncertainties in the velocity model using a variation in velocity with a standard deviation of 5%. The average of the P and S-wave magnitudes for the events ranges between -0.8 and 1.7 but the differences between estimates using P- and S-arrivals can be up to ~1.0 units (Fig. 12). This variation is thought to be mainly attributable to the average radiation pattern correction used because the difference between the P- and S-estimates varies with azimuth (Fig. 12) and Stork et al. (2014) have shown that the use of average radiation pattern correction terms can cause such uncertainties.

An important question in any CCS project is, what is the maximum magnitude earthquake that may be triggered? Assuming a circular source model with radius d, the stress drop, derived from Eshelby (1957), is

$$\Delta\sigma_s = \frac{7M_0}{16d^3}. \tag{2}$$

Assuming events with $\Delta\sigma_s$ between 0.1 MPa and 10 MPa (e.g., Abercrombie, 1995) and a maximum fracture radius of 100 m (Iding and Ringrose, 2010), we estimate the maximum expected moment magnitude from the pre-existing fractures to be between 1.6 and 2.9. This is similar to our reported maximum magnitude of 1.7 and we therefore suggest that seismic activity with magnitudes up to ~2 could have been reasonably expected before CO_2 injection began.

The Gutenberg–Richter relationship, $\log_{10}N = a - bM$ where N is the number of earthquakes greater than magnitude M, is the commonly assumed frequency of occurrence distribution of earthquake magnitudes and is often used to characterise earthquake generation. The b-value, the slope of the frequency-magnitude distribution, is globally found to be ~1.0 but larger b-values have been estimated up to ~2.0 in volcanic regions and where fluid injection increases pore pressure and causes fracturing (McNutt, 2005; Bachmann et al., 2012; Eaton et al., 2014). We thus estimate b-values for the In Salah data to test whether there is any variation in event generation with injection rates, over time or with event location. We use the maximum likelihood method (Aki, 1965) to find b and apply a Kolmogorov–Smirnoff test to find the completeness magnitude. To estimate the standard error in b we use the formulae given by Shi and Bolt (1982). Overall, we find $b = 2.17 \pm 0.09$ for average P- and S-wave magnitudes with a magnitude of completeness of 0.1. This is a very high b-value but similar to the values reported by other studies of fluid injection sites, for example during hydraulic fracturing (Maxwell et al., 2009) and at Enhanced Geothermal System (EGS) injections (Bachmann et al., 2012). However, looking at the data in more detail reveals that the b-value is dependent on the station-source azimuth, rather than the injection rate. Events to the WNW of the array have b-values much closer to 1.0 (1.47 ± 0.13; Fig. 13a) and events to the ESE occur with a very high b-value (2.46 ± 0.18; Fig. 13b). As a consequence of using average radiation pattern corrections to estimate M_w the b-value is unreliable and depends on azimuth. However, the b-values estimated here are all high (>1.4), and since Cluster 2 occurs within a short ($\lesssim 1.0$ km) horizontal distances from the injection site, it is likely that pore pressures are elevated in this area by the presence of CO_2, thus resulting in a proportionally large number of small magnitudes events.

Our reported b-values for events to the WNW of the array are similar to the values reported by Goertz-Allmann et al. (2014) (their clusters named B and D). For events to the ESE we find a larger b-value (2.5 compared to 1.7–1.9 reported by Goertz-Allmann et al., 2014 for their Cluster C). As stated above, M_w estimates may have errors up to 1.0 units if only one instrument is available to make the estimate due to uncertainties in radiation pattern corrections; the time windows selected around the arrival; and uncertainties in event location, velocities and attenuation (e.g., Stork et al., 2014). In particular we believe the estimated magnitudes of the events to the ESE of the array are unreliable because there is poor agreement between the values obtained from P- and S-arrivals. The differences in magnitudes and b-values between this study and that by Goertz-Allmann et al. (2014) reflect the uncertainties in the magnitude estimates.

4.5. Fracture strike and density using shear-wave splitting

Anisotropic seismic wave velocities arise in rock with aligned fracture sets with sizes and spacing smaller than the
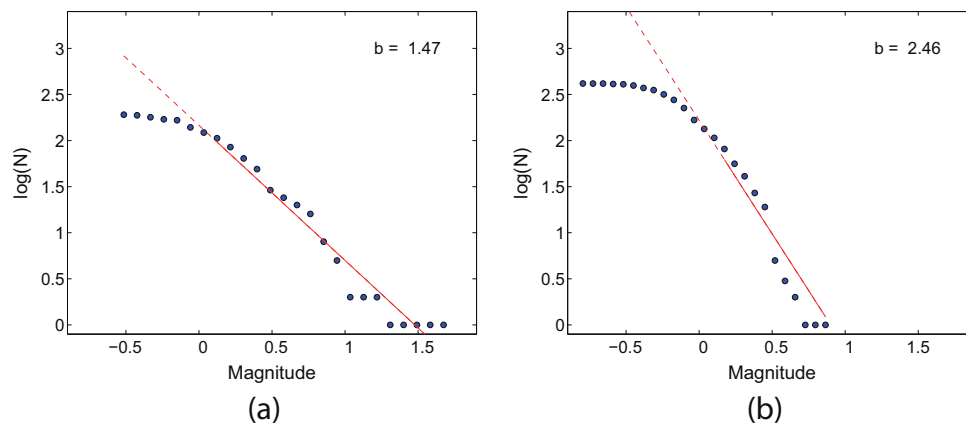
Fig. 13. *b*-Values estimated for events (a) with station-source azimuths 270°–310°, (b) with station-source azimuths 90°–130°.

dominant wavelength (e.g., Hudson, 1980). Characterisation of this anisotropy can therefore be used to infer fracture properties and to this end shear-wave splitting analysis has been successfully applied in hydrocarbon recovery and mining settings to determine fracture strike, density and compliance ratios (e.g., Wuestefeld et al., 2011; Verdon and Wüstefeld, 2013; Baird et al., 2013). Temporal variations in these characteristics provide important useful information to operators regarding fluid flow behaviour and the potential for cavity collapse events. We therefore apply the automated approach to shear-wave splitting analysis of Wuestefeld et al. (2010) to confirm previously reported fracture orientations and to look for any evidence of changes in the orientation or density of the fractures with CO_2 injection. This method computes splitting parameters, the strike of the fast polarisation direction, Φ, and the time delay between the fast and slow *S*-waves, δt, using both the cross-correlation (e.g., Bowman and Ando, 1987) and eigenvalue (e.g., Silver and Chan, 1991) methods. A measurement is deemed "good" using a quality index relying on the similarity of the results of the two methods, as described in Wuestefeld et al. (2010).

For all events with *S*-wave picks we estimate Φ, as a measure of the dominant fracture direction, and δt, as a measure of the degree of anisotropy. For quality control we require a quality index of >0.8 and an estimated error in $\Phi < 5°$ and we then inspect the results by hand. This leads to 349 "good" results and an example result is shown in Fig. 14. Fig. 14b and c highlights the advantage of using two methods to compute shear-wave splitting parameters since the cross-correlation results (Fig. 14c) show evidence of cycle skipping which could lead to the wrong δt being reported. Fig. 15 shows the Φ and δt estimated for the 349 good results and the noticeable feature of Fig. 15a is the consistency of strike of the fast direction NW-SE. This provides an estimate of the dominant fracture strike, 140°–160°, that is consistent with the results from logging data (Iding and Ringrose, 2010) and fracture modelling (Bond et al., 2013). Although the lower limit of delay time measurements remains constant at ~0.030 s between 2009 and 2011, the upper limit during periods of high injection increases to 0.10 s. The events with larger delay times originate mainly from east of the monitoring well (red colours in Fig. 15b) Once injection rates decrease, towards the end of 2010, the upper limit for delay times returns to 0.05 s. This may indicate that high injection rates are opening pre-existing fractures around the injection well, resulting in an apparent increase in fracture density, that then close following the migration of CO_2 through the fractures. These results do not rule out the possibility that injection prior to August 2009 created new fractures or that fractures were created after August 2009 that these raypaths do not sample.

5. Discussion

5.1. Importance of experimental set-up

The microseismic data from the In Salah CCS site should be influential in the planning of future CCS projects in terms of how a site is monitored. The project was the first non-EOR >1 Mt storage project to be monitored by a microseismic array and the results presented above prove the usefulness of the data in understanding the geomechanical response of the site to CO_2 injection. The main advantage of microseismic monitoring over other geophysical techniques, such as 4D seismic reflection and InSAR, is that the data can be processed in real-time and therefore analysis can provide an early warning system for CO_2 leakage or fault reactivation.

Unfortunately, due to the set-up of the pilot microseismic array at In Salah, the information to be gained from this dataset is limited. The main influence on the certainty of the results presented above is the fact that only one 3-C geophone could be used in the analysis. Accurate seismic event locations require multi-sensor arrays (>5 instruments) covering a wide aperture, allowing a detailed analysis of which structures are being activated. However, we have shown that even a shallow microseismic array could be useful to monitor the geomechanical response of CCS sites. With one instrument and using particle motion analysis we are able to constrain approximate locations for some events and make observations of fracture properties. We suggest that the repeating events in the clusters occur along the NW-SE oriented pre-existing fracture zone with events occurring on neighbouring fractures with very similar orientations, hence the similarity in waveforms and t_{sp} times within the clusters. A schematic form of our interpretation in Fig. 16 illustrates our inferred event epicentres and how fractures in the pre-existing fracture zone are expected to open preferentially because they are aligned with the present day direction of maximum horizontal stress. However, we are unable to report accurate locations for the events and our modelling and ray-tracing results suggest that our locations estimated from the grid search could be in error by up to ~200 m horizontally due to the discretisation of the grid and up to ~500 m horizontally if the measured inclination is out by 5° (Fig. 9). Additionally, the depths could be in error by ~400 m if there are errors up to 10% in the velocity model.

Recently, some methods for single-station experiments have been developed although these require specific set-ups, such as significant coda waves recorded for highly correlated waveforms from clusters of earthquakes (Robinson et al., 2013). When a CCS project is undertaken a microseismic array should be deployed that can be used to track the CO_2 footprint using any seismic activity and also that is able to detect unexpected seismic activity at some
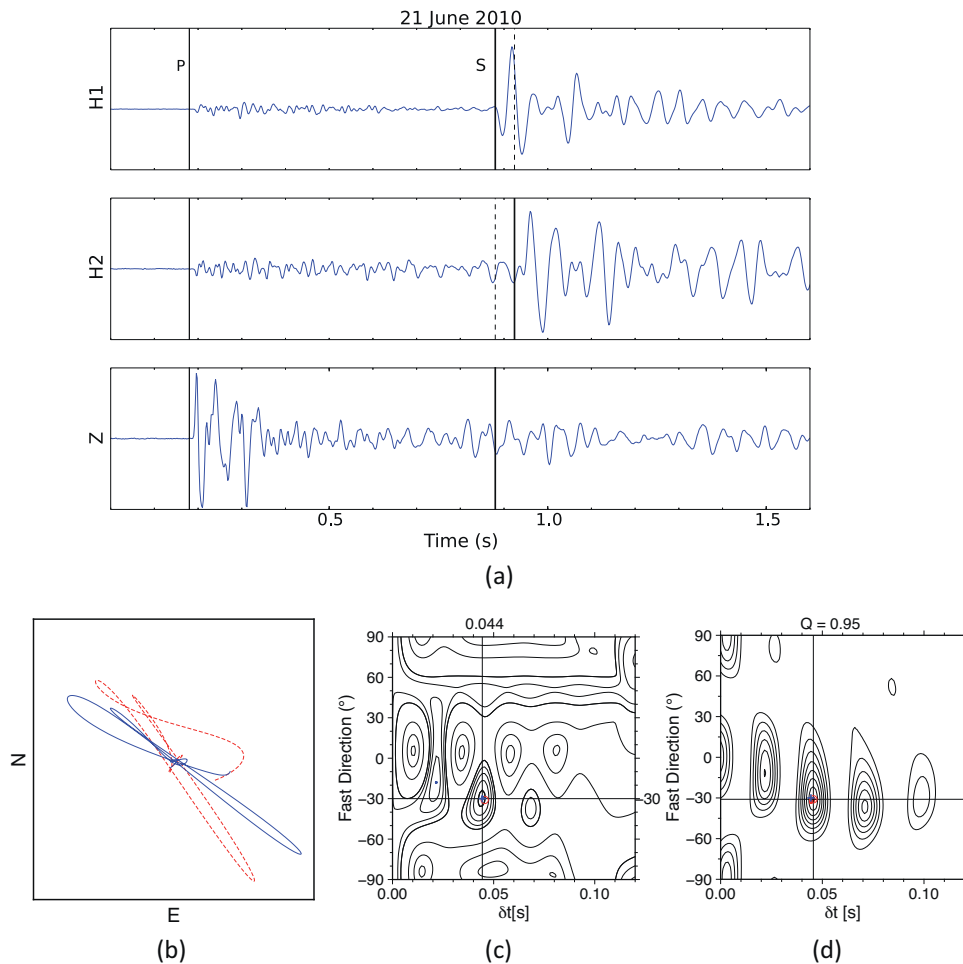
Fig. 14. (a) Example 3C waveforms for an event with a split S-wave. The two horizontal (H1 and H2) and the vertical (Z) components are shown. (b) The particle motion in SH-SV coordinates before (dashed red line) and after (blue line) correction. Note the motion is linearly polarised after correction. (c) Map of error surfaces for the eigenvector method. The best-fitting delay time and fast direction are shown. (d) Map of error surfaces for the cross-correlation method. The combined quality value, Q, for the two methods is shown. The blue cross and red circle in (c) and (d) indicate the best fitting results from the two methods. (For interpretation of the references to color in this figure legend, the reader is referred to the web version of this article.)

distance from the injection point. For an overview of recommendations for microseismic array deployments at CCS sites see Verdon et al. (2012).

Good coverage of the focal sphere also allows the computation of focal mechanism solution and hence an understanding of the type of deformation taking place. With the available data from In Salah we are unable to do this with any confidence. Since we do not know the focal mechanism solutions our estimates of M_w may be in error up to 1.0 unit (Stork et al., 2014). The recording frequency of 500 Hz also affects our magnitude estimates since we cannot determine Q from the source spectra because the corner frequencies for such small earthquakes could be around the Nyquist frequency for this data. If Q is to be estimated from source spectra it is recommended that the recording frequency is at least 4 times the Nyquist frequency (McGarr, 1984; Baig and Urbancic, 2010).

Finally, the pilot microseismic monitoring array at In Salah was deployed 5 years after injection began. It is therefore impossible to assess the true impact of CO_2 injection even with a perfectly designed array because the data cannot be compared to a baseline taken before injection began. Even so, the microseismic, 3D seismic and InSAR monitoring clearly revealed how CO_2 injection was affecting the site, acting as an early warning system to ensure the response could be controlled. This should provide confidence in moving forward with other CCS sites, as long as appropriate monitoring is in place. We therefore recommend that a suitable

microseismic array is installed at future CCS sites prior to the start of injection activities.

5.2. Combining microseismic and geomechanical studies

It is important that any microseismic observations are combined with geomechanical studies to verify the site response predicted by geomechanical models. Verdon et al. (in preparation) combine a history matched reservoir model that simulates pore pressure changes caused by gas extraction and CO_2 injection with a fracture model to determine when and where Mohr–Coulomb failure criteria were exceeded. This is verified against the results from this study to understand the changes in the rate and location of seismicity at the In Salah site through time. Such combined studies will improve with developments in computing power and increased complexity of models, with improved instrumentation and appropriate deployments of microseismic arrays. These types of studies are essential for future projects to fully understand how sites react to CO_2 injection.

Recently, White et al. (2014) consider the evidence for different explanations for the observed geomechanical response at In Salah. They conclude that the most likely explanation for the observed surface deformation, seismic and pressure data is that the lowermost caprock was hydrofractured by CO_2 injection and that preexisting fractures could play a significant role. Our
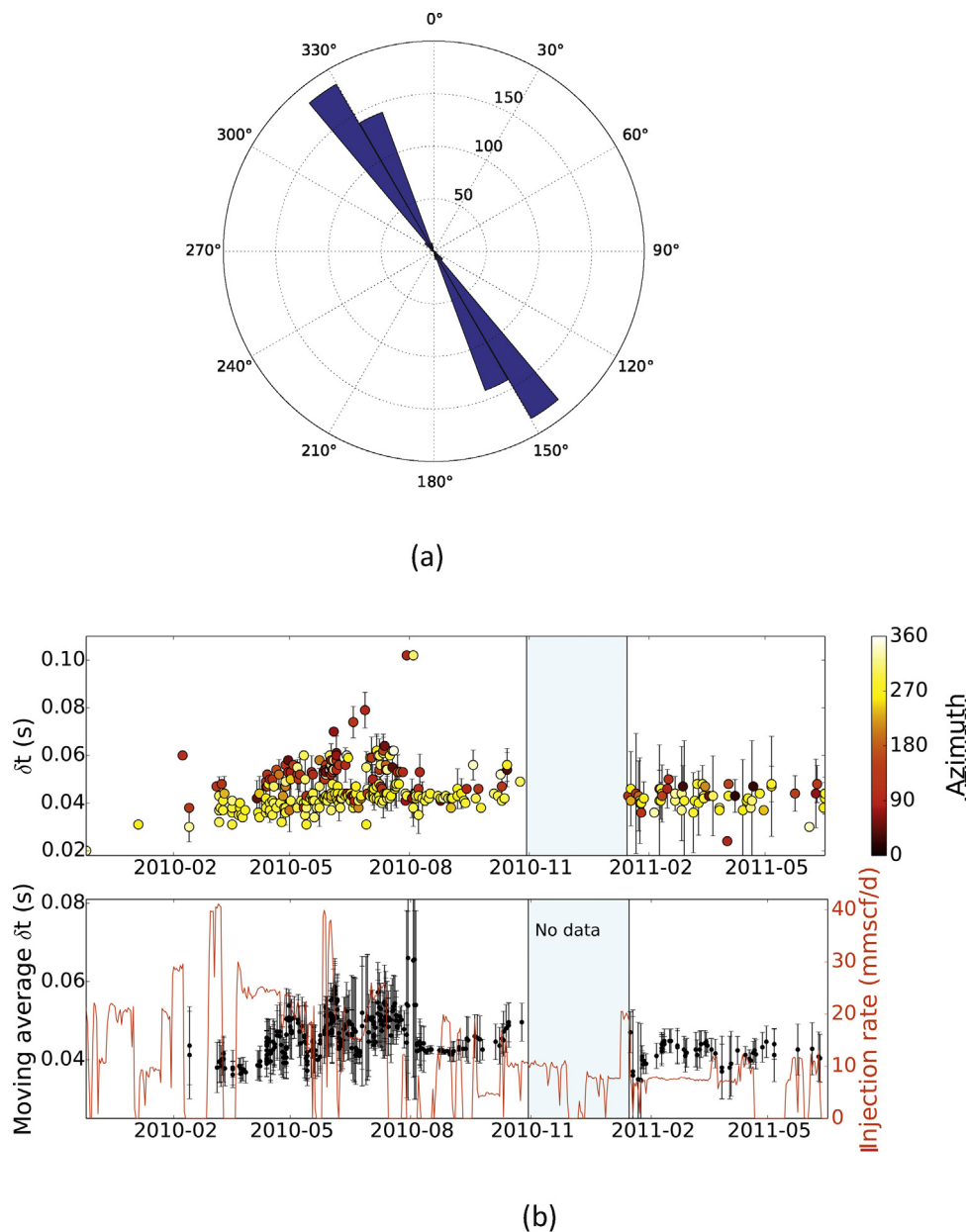
(a)

(b)

Fig. 15. (a) Histogram of the strike of the fast shear-wave. (b) Upper panel: Delay time, δt, between the fast and slow shear-waves as a function of time, measured using automated shear-wave splitting analysis. Lower panel: The red line is the CO_2 injection rate and the black line is the 5 point moving average of δt values. (For interpretation of the references to color in this figure legend, the reader is referred to the web version of this article.)

shear-wave splitting observations, made towards the end of the injection period, support the idea that preexisting fractures are being reactivated at this time.

Comparing and contrasting this study with that of Goertz-Allmann et al. (2014) shows many similarities but key differences. The method used to pick arrival times significantly affects the number of microseismic events identified (compare this study with Oye et al. (2013) and Goertz-Allmann et al. (2014)). In the present study we find more but less tightly clustered events. This may be because our picking method does not rely on a correlation between events, only between receivers. We observe similar variations in event rate, magnitudes and b-values to the aforementioned studies. Small discrepancies between the studies may be put down to differences in processing techniques. However, in contrast to the study of Goertz-Allmann et al. (2014) we observe variations in the delay time between fast and slow shear-waves dependent on the injection rate. This leads us to conclude that the injection is

opening preexisting fractures around the injection well that then close as pressure reduces. This is an important difference in the conclusions of the two studies. Overall, we find smaller delay times than those reported by Goertz-Allmann et al. (2014) but we find similar results for events in our Cluster 1 (their Cluster A). The differences between the inferred dominant fracture strike are more difficult to explain. Our reported orientation (NW-SE) is in agreement with fracture orientations derived from logging data (Iding and Ringrose, 2010) and the regional maximum horizontal stress. The difference between the studies may be because we report results for different events, both studies report results from <5% of the total events detected.

5.3. Comparison with other CCS sites

The large number of events detected at the In Salah site is in contrast to the very few events (~100) that were detected at
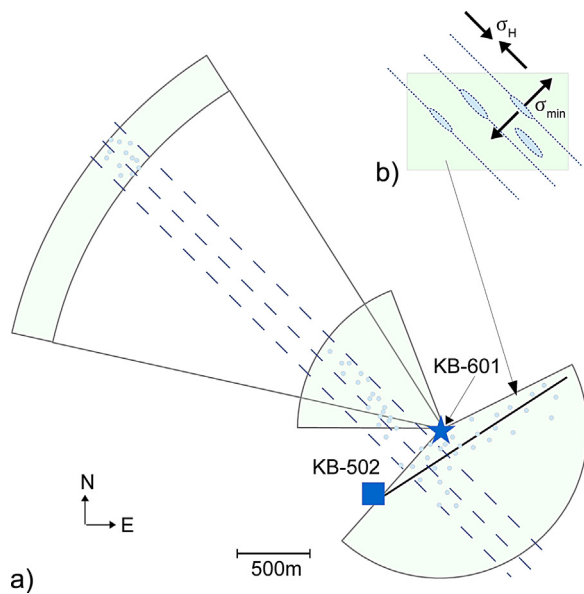
Fig. 16. (a) Schematic illustration of the interpreted locations of microseismic events (circles) detected by the microseismic array in well KB-601 (star). Injection well KB-502 is marked by the square and the horizontal extent of this well by the thicker black line. The dashed line is the estimated location of the reported fracture zone. The green areas are the areas containing events according to our observations and modelling results. (b) A magnified image of the events in the fracture zone aligned with the direction of maximum horizontal stress, σ_H, and a representation of pre-existing fractures opening in the direction of minimum horizontal stress, σ_{min}, during CO_2 injection. (For interpretation of the references to color in this figure legend, the reader is referred to the web version of this article.)

Weyburn (Verdon et al., 2011), a large-scale CCS-EOR project that has been studied using microseismic data. Despite substantial differences in physical properties (e.g., porosity and permeability) and geomechanical response between major CCS sites (see Eiken et al., 2011; Verdon et al., 2013) each site successfully stores CO_2 and to-date there has been no leakage reported at any site storing >1 Mt of CO_2. The significant microseismic activity recorded by the In Salah array does not necessarily imply that CO_2 is leaking into the caprock formation, and this is why it would be very beneficial to understanding the site to be able to compute accurate and precise event locations. The study by Verdon et al. (2011) uses geomechanical modelling to understand seismicity produced through stress transfer rather than directly by fluid movement at the Weyburn site. The few events with t_{sp} < 0.5 observed in this study could result from similar effects. These observed differences between CCS sites highlight why it is important that each potential CCS site should be carefully characterised and monitored to understand and verify safe CO_2 storage.

6. Conclusion

Our observation and analysis of microseismicity recorded at the In Salah CO_2 sequestration site exhibits little variation in characteristics throughout the monitoring period, 2009–2011. Although thousands of events are recorded, they occur in clusters with similar waveforms and apparently collocated hypocentres. Shear-wave splitting analysis implies the rays are sampling fractures oriented predominantly NW-SE. This is consistent with the observations of the pre-existing dominant fracture orientation reported from borehole logging data. The maximum estimated moment magnitude of M_W = 1.7 is also consistent with the fracture dimensions estimated from the borehole data. There is some evidence from an increase in shear-wave splitting delay times that pre-existing fractures are opening in close proximity to the injection well during

periods of high CO_2 injection rates, thereby increasing the degree of anisotropy. The delay times return to the original values when injection rates fall, indicating a closure of fractures as pressure reduces.

This body of evidence points to a predictable microseismic response to the injection of CO_2 at well KB-502. Even though the instrumental set-up and data reliability place constraints on the conclusions we are able to draw from the microseismic data, our analysis shows that events are likely occurring along a pre-existing NW-SE oriented fracture zone close to the injection well. High b-values (1.4–2.5) suggest that fluids are lubricating this fracture zone, resulting in large numbers of small magnitude events. Relative to other major CO_2 injection sites, the site at In Salah has low porosity and permeability but the results of this and other geophysical studies indicate that the injected volume is accommodated by and confined to the fracture zone in the reservoir and lowermost caprock, rather than creating or reactivating shallower fractures to create pathways for CO_2 to migrate to the surface. We also note that when injection ceases the rate of seismic events drops quickly <10 events/day. It is reassuring to operators if seismicity can be controlled in this way.

Unfortunately microseismic monitoring began at the In Salah storage site five years after CO_2 injection and therefore the results and conclusions are based on data recorded 2009–2011. We do not make any assertions regarding the microseismicity or fracture characteristics before August 2009. It is an important point for future projects that, with baseline microseismic data and monitoring when injection began, it would have been possible to gain a much fuller understanding of the geomechanical response of the site to CO_2 injection and it is likely that microseismic data would have highlighted the activation of the fracture zone before it could be detected using other techniques, such as InSAR. Despite the limitations of this microseismic dataset, the small number of instruments and restricted monitoring period, this study shows that useful information can be gained from the data to help regulate injection parameters and thus the response of the site CO_2 injection.

References

Abercrombie, R., 1995. Earthquake source scaling relationships from −1 to 5 m_L using seismograms recorded at 2.5-km depth. J. Geophys. Res. 100 (B12), 24015–24036.

Aki, K., 1965. Maximum likelihood estimate of b in the formula $logN = a − bM$ and its confidence limits. Bull. Earthquake Res. Inst 43, 237–239.

Bachmann, C.E., Wiemer, S., Goertz-Allmann, B.P., Woessner, J., 2012. Influence of pore-pressure on the event-size distribution of induced earthquakes. Geophys. Res. Lett. 39, L09302.

Baig, A., Urbancic, T., 2010. Magnitude determination, event detectability, and assessing the effectiveness of microseismic monitoring programs in petroleum applications. CSEG Rec. 35, 22–26.

Baird, A., Kendall, J.-M., Verdon, J., Wuestefeld, A., Noble, T., Li, Y., Dutko, M., Fisher, Q., 2013. Monitoring increases in fracture connectivity during hydraulic stimulations from temporal variations in shear wave splitting polarization. Geophys. J. Int. 195, 1120–1131.

Bond, C., Wightman, R., Ringrose, P., 2013. The influence of fracture anisotropy on CO_2 flow. Geophys. Res. Lett 40, 1–6.

Boore, D., Boatwright, J., 1984. Average body-wave correction coefficients. Bull. Seis. Soc. Am 74, 1615–1621.

Bowman, J., Ando, M., 1987. Shear-wave splitting in the upper-mantle wedge above the Tonga subduction zone. Geophys. J. Roy. Astr. Soc 88, 25–41.

Chadwick, R.A., Williams, G.A., Williams, J.D.O., Noy, D.J., 2012. Measuring pressure performance of a large saline aquifer during industrial-scale CO_2 injection: the Utsira Sand, Norwegian North Sea. Int. J. Greehouse Gas Control 10, 374–388.

Claassen, J., 2001. Robust bearing estimation for three-component stations. Pure Appl. Geophys 158, 349–374.

Coueslan, M., Smith, V., Jaques, P., Will, R., Maxwell, S., Raymer, D., Senel, O., Finley, R., 2013. Evolution of induced microseismicity at the Illinois Basin – Decatur project. In: AGU Fall Meeting (S23E-02).

De Meersman, K., van der Baan, M., Kendall, J.-M., 2006. Signal extraction and automated polarization analysis of multicomponent array data. Bull. Seis. Soc. Am. 96, 2415–2430.

Delépine, N., Cuenot, N., Rothert, E., Parotidis, M., Rentsch, S., Shapiro, S., 2004. Characterization of fluid transport properties of the Hot Dry Rock reservoir Soultz-2000 using induced microseismicity. J. Geophys. and Eng. 1, 77–83.

Eaton, D.W., Davidsen, J., Pedersen, P.K., Boroumand, N., 2014. Breakdown of the Gutenberg–Richter relation for microearthquakes induced by hydraulic fracturing: influence of stratabound fractures. Geophys. Prospect. 62, 806–818.

Eiken, O., Ringrose, P., Hermanrud, C., Nazarian, B., Torp, T.A., Høier, L., 2011. Lessons learned from 14 years of CCS operations: Sleipner, In Salah and Snøhvit. Energy Proc. 4, 5541–5548.

Eshelby, J., 1957. The determination of the elastic field of an ellipsoidal inclusion, and related problems. Proc. R. Soc. London 241, 376–396.

Forghani-Arani, F., Behura, J., Haines, S.S., Batzle, M., 2013. An automated cross-correlation based event detection technique and its application to a surface passive data set. Geophys. Prospect. 61, 778–787.

Goertz-Allmann, B.P., Kühn, D., Oye, V., Bohloli, B., Aker, E., 2014. Combining microseismic and geomechanical observations to interpret storage integrity at the In Salah CCS site. Geophys. J. Int. 198, 447–461.

Hudson, J., 1980. Overall properties of a cracked solid. In: Mathematical Proceedings of the Cambridge Philosophical Society, vol. 88, pp. 371–384.

Iding, M., Ringrose, P., 2010. Evaluating the impact of fractures on the performance of the In Salah CO_2 storage site. Int. J. Greenhouse Gas Control 4, 242–248.

Kaiser, E., 1959. A study of acoustic phenomena in tensile test. TH München, Munich, Germany, Ph. D. thesis.

Kendall, J.-M., Thomson, C.J., 1989. A comment on the form of the geometrical spreading equations, with some numerical examples of seismic ray tracing in inhomogeneous, anisotropic media. Geophys. J. Int. 99, 401–413.

Larsen, S., Grieger, J., 1998. Elastic modeling initiative, Part III: 3-D computational modeling. SEG Expand. Abstr. 68, 1803–1806.

Mathieson, A., Midgley, J., Dodds, K., Wright, I., Ringrose, P., Saoula, N., 2010. CO_2 sequestration monitoring and verification technologies applied at Krechba, Algeria. Lead. Edge 29, 216–222.

Mathieson, A., Midgley, J., Wright, I., Saoula, N., Ringrose, P., 2011. In Salah CO_2 Storage JIP: sequestration monitoring and verification technologies applied at Krechba, Algeria. Energy Proc. 4, 3596–3603.

Maxwell, S., Jones, M., Parker, R., Miong, S., Leaney, S., Dorval, D., D'Amico, D., Logel, J., Anderson, E., Hammermaster, K., 2009. Fault activation during hydraulic fracturing. SEG Expand. Abstr., 1552–1556.

Maxwell, S., Urbancic, T., Demerling, T., Prince, M., 2002. Real time 4D seismic imaging of hydraulic fractures. In: SPE/ISRM78191.

McGarr, A., 1984. Scaling of ground motion parameters, state of stress, and focal depth. J. Geophys. Res. 89 (B8), 6969–6979.

McNutt, S., 2005. Volcanic seismology. Annu. Rev. Earth Planet. Sci. 33, 461–491.

Orlecka-Sikora, B., Papadimitriou, E., G, K., 2009. A study of the interaction among mining-induced seismic events in the Legnica-Głogów Copper District, Poland. Acta Geophys. 57, 413–434.

Oye, V., Aker, E., Daley, T.M., Kühn, D., Bahman, B., Korneev, V., 2013. Microseismic monitoring and interpretation of injection data from the In Salah CO_2 storage site (Krechba), Algeria. Energy Proc. 37, 4191–4198.

Ringrose, P., Atbi, M., Mason, D., Espinassous, M., Myhrer, Ø., Iding, M., Mathieson, A., Wright, I., 2009. Plume development around well KB-502 at the In Salah CO_2 storage site. First Break 27, 85–89.

Ringrose, P.S., Mathieson, A.S., Wright, I.W., Selamac, F., Hansen, O., Bissell, R., Saoula, N., Midgley, J., 2013. The In Salah CO_2 storage project: lessons learned and knowledge transfer. Energy Proc. 37, 6226–6236.

Robinson, D.J., Sambridge, M., Snieder, R., J., H., 2013. Relocating a cluster of earthquakes using a single seismic station. Bull. Seis. Soc. Am. 103, 3057–3072.

Rucci, A., Vasco, D.W., Ferretti, A., 2013. Monitoring the geologic storage of carbon dioxide using multicomponent SAR interferometry. Geophys. J. Int. 193, 197–208.

Rutqvist, J., 2012. The geomechanics of CO_2 storage in deep sedimentary formations. Geotech. Geol. Eng. 30, 525–551.

Schoenball, M., Baujard, C., Kohl, T., Dorbath, L., 2012. The role of triggering by static stress transfer during geothermal reservoir stimulation. J. Geophys. Res. 117, B09307.

Shi, Y., Bolt, B.A., 1982. The standard error of the magnitude-frequency b value. Bull. Seis. Soc. Am. 72, 1677–1687.

Silver, P., Chan, W., 1991. Shear wave splitting and subcontinental mantle deformation. J. Geophys. Res. 96 (B10), 16429–16454.

Stork, A.L., Verdon, J.P., Kendall, J.-M., 2014. The robustness of seismic moment and magnitudes estimated using spectral analysis. Geophys. Prospect. 62, 862–878.

Stork, A.L., Verdon, J.P., Kendall, J.-M., 2015. Assessing the effect of velocity model accuracy on microseismic interpretation at the in Salah Carbon Capture and Storage site. Energy Proc.

Vasco, D.W., Rucci, A., Ferretti, A., Novali, F., Bissell, R.C., Ringrose, P.S., Mathieson, A.S., Wright, I.W., 2010. Satellite-based measurements of surface deformation reveal fluid flow associated with the geological storage of carbon dioxide. Geophys. Res. Lett. 37, L03303.

Verdon, J., Kendall, J.-M., D.J., W., 2012. Monitoring carbon dioxide storage using passive seismic techniques. In: Proceedings of the Institution of Civil Engineers, Energy, vol. 165, pp. 85–89.

Verdon, J.P., 2014. Significance for secure CO_2 storage of earthquakes induced by fluid injection. Env. Rev. Lett 9, 064022.

Verdon, J.P., Kendall, J.-M., Stork, A.L., Chadwick, R.A., White, D.J., Bissell, R.C., 2013. Comparison of geomechanical deformation induced by megatonne-scale CO_2 storage at Sleipner, Weyburn, and In Salah. PNAS 110, E2762–E2771.

Verdon, J.P., Kendall, J.-M., White, D.J., Angus, D.A., 2011. Linking microseismic event observations with geomechanical models to minimise the risks of storing CO_2 in geological formations. Earth Planet. Sci. Lett. 305, 143–152.

Verdon, J.P., Stork, A.L., Bissell, R.C., Bond, C.E., Werner, M.J., in preparation. Simulation of seismic events induced by CO_2 injection at In Salah, Algeria.

Verdon, J.P., Wüstefeld, A., 2013. Measurement of the normal/tangential fracture compliance ratio ($Z_N Z_T$) during hydraulic fracture stimulation using S-wave splitting data. Geophys. Prospect. 61 (Suppl. 1), 461–475.

White, J., Chiaramontea, L., Ezzedineb, S., Foxalla, W., Haoa, Y., Ramireza, A., McNab, W., 2014. Geomechanical behavior of the reservoir and caprock system at the In Salah CO_2 storage project. PNAS 111, 8747–8752.

Wuestefeld, A., Al-Harrasi, O., Verdon, J., Wookey, J., Kendall, J.-M., 2010. A strategy for automated analysis of passive microseismic data to image seismic anisotropy and fracture characteristics. Geophys. Prospect. 58, 755–773.

Wuestefeld, A., Kendall, J.-M., Verdon, J.P., van As, A., 2011. In situ monitoring of rock fracturing using shear wave splitting analysis: an example from a mining setting. Geophys. J. Int 187, 848–860.

Zoback, M.D., Gorelick, S.M., 2012. Earthquake triggering and large-scale geologic storage of carbon dioxide. PNAS 109, E3624–E3624.